Published: 12th May 2026

ANACHEM JOURNAL
ISSN: 2006-5221 (Online)

ADSORPTIVE REMOVAL AND KINETIC MODELLING OF COLOUR, TURBIDITY, AND COD FROM SLAUGHTERHOUSE WASTEWATER USING BIOSYNTHESIZED SILVER NANOPARTICLES FROM AQUEOUS EXTRACT OF PINEAPPLE PEEL (*Ananas Comosus)*

[1*]Obiadi, C. M., [1]Iloamaeke, I.M., and [1]Okonkwo, C.P.
[1]Department of Pure and Industrial Chemistry, Nnamdi Azikiwe University, Awka, Anambra State, Nigeria.
*Corresponding author's e-mail: mc.obiadi@unizik.edu.ng
DOI: **https://doi.org/10.5281/zenodo.20128534**

ABSTRACT

This study investigates the adsorptive removal and kinetic modelling of colour, turbidity, and chemical oxygen demand (COD) from slaughterhouse wastewater (SWW) using silver nanoparticles (AgNPs) biosynthesized from the aqueous extract of pineapple peel (Ananas comosus); designated AgPPE. AgPPE were synthesized, characterized by UV–Vis spectroscopy, Fourier-transform infrared spectroscopy (FTIR), transmission electron microscopy (TEM), X-ray diffraction (XRD), energy-dispersive X-ray spectroscopy (EDX), and Brunauer–Emmett–Teller (BET) surface area analysis. TEM revealed spherical nanoparticles of a mean diameter of 14.62 to 17.63 nm; XRD confirmed face-centred cubic metallic silver; The surface area of the BET was 449.842 m2 / g. Batch adsorption experiments were conducted, achieving adsorption efficiencies of 75.18% (Colour), 72.94% (Turbidity), and 71.27% (COD). Pseudo-second-order kinetic modelling provided the best fit ($R^2 \geq 0.9997$), indicating chemisorption as the dominant mechanism. Intraparticle diffusion was involved but was not the sole rate-controlling step, as confirmed by Boyd plot analysis. The findings demonstrate that biogenic AgPPE is an effective, low-cost, and eco-friendly nanomaterial for the remediation of slaughterhouse wastewater.

Keywords: Adsorption kinetics; COD removal; Decolourisation; Silver Nanoparticles; Slaughterhouse Wastewater; Turbidity Removal.

1.0. Introduction

Water scarcity and pollution are among the most pressing environmental challenges facing the world in the twenty-first century (Mekonnen & Hoekstra, 2016). Among the most recalcitrant categories of industrial effluent is wastewater generated from slaughterhouse and abattoir operations, which presents an exceptionally complex pollution burden due to its inherent mixture of blood, fats, proteins, suspended solids, pathogens and recalcitrant organic compounds (Aziz et al., 2019). The global livestock sector processes billions of animals annually, generating correspondingly enormous volumes of wastewater that, when inadequately managed, impose severe ecological and public health consequences (Food and Agriculture Organisation (FAO), 2022; Bustillo-Lecompte & Mehrvar, 2015).

Slaughterhouse wastewater (SWW) is characteristically high in biological oxygen

demand (BOD), chemical oxygen demand (COD), turbidity, colour, and total suspended solids (TSS), while also harbouring elevated concentrations of nitrogen, phosphorus, and potentially pathogenic microorganisms (Bustillo-Lecompte & Mehrvar, 2015). The discharge of untreated or inadequately treated SWW into receiving water bodies, a practice regrettably common in many developing nations, including Nigeria, degrades aquatic ecosystems through oxygen depletion, eutrophication, pathogen contamination, and aesthetic deterioration (Eze & Eze, 2018). Colour and turbidity, though often perceived as aesthetic parameters, exert tangible ecological impacts by attenuating light penetration, disrupting aquatic photosynthesis, and signalling the presence of dissolved and colloidal organic matter that may be biologically recalcitrant (Ang & Mohammad, 2020; Rehman et al., 2019). COD, as a global measure of the oxygen demand imposed by oxidisable matter in wastewater, serves as a robust surrogate for the organic pollution load; therefore, its reduction is a primary treatment objective (Ahmed et al., 2021).

Conventional wastewater treatment technologies, including coagulation-flocculation, biological treatment of activated sludge, membrane filtration, and chlorination, are effective but suffer from well-documented limitations: high capital and operational costs, secondary sludge generation requiring further management, limited efficacy against recalcitrant organics, and unsuitability for small-scale or rural installations (Crini & Lichtfouse, 2019). These shortcomings have motivated extensive research into alternative and cost-effective treatment technologies, among which adsorption has emerged as particularly promising due to its operational simplicity, design flexibility, low energy requirement, and ability to achieve high removal efficiencies even at low pollutant concentrations (Crini et al., 2019; Al-Ghouti & Da'ana, 2020).

Nanomaterials have transformed the landscape of water and wastewater treatment due to their extraordinarily high surface-area-to-volume ratios, tunable surface chemistry, and unique physico-chemical properties not exhibited by their bulk counterparts (Lu & Astruc, 2018; Jain et al., 2021). Among the diverse portfolio of engineered nanomaterials, silver nanoparticles (AgNPs) occupy a prominent position due to their documented multifunctionality: potent broad-spectrum antimicrobial activity, catalytic capacity for the degradation of organic pollutants, and substantial adsorptive capacity for dyes, heavy metals, and other organic contaminants (Zhang et al., 2016). Antimicrobial functionality is particularly consequential in the context of SWW treatment, where pathogen inactivation is simultaneously desirable alongside pollutant removal (Deshmukh et al., 2019).

Conventional chemical synthesis of AgNPs, while effective, relies on hazardous reducing agents such as sodium borohydride, toxic stabilising surfactants, organic solvents, and energy-intensive procedures, all of which compromise environmental sustainability and impose high economic costs (Abid et al., 2022; Güzel & Erdal, 2018). This has catalysed the rapid growth of green or biogenic synthesis approaches, in which plant extracts, microbial cultures, or agricultural by-products supply both the reducing and capping agents for nanoparticle formation in a single-step, ambient-conditions, chemically benign process (Ahmed et al., 2016). Green synthesis aligns with the principles of sustainable chemistry by eliminating toxic reagents, minimizing waste, and valorising agricultural by-products into value-added nanomaterials (Rocha et al., 2024).

Pineapple (Ananas comosus [L.]) is one of the most economically significant tropical fruits worldwide, ranking among the top three most consumed tropical fruits worldwide (FAO, 2022). The post-harvest processing of pineapple generates a substantial volume of

peel residues that comprise approximately 25-35% of the total fruit mass and are routinely discarded or underutilised, representing both an economic loss and a potential environmental burden (Yusoff et al., 2020). Pineapple peel is, however, compositionally rich in a diverse array of phytochemicals with strong reducing and chelating capacity: polyphenols (ferulic acid, caffeic acid, p-coumaric acid, chlorogenic acid), flavonoids (quercetin, luteolin, naringenin), ascorbic acid, and the distinctive cysteine protease bromelain, along with structural polysaccharides (pectin, cellulose, hemicellulose) (Mohammed et al., 2017; Yusoff et al., 2020). These phytochemicals collectively endow the aqueous pineapple peel extract with the dual capacity to reduce Ag^{+} ions to Ag^{0} and to cap/stabilise the resulting nanoparticles; the two fundamental requirements for a plant extract-mediated bioreduction synthesis (Das et al., 2019; Baran et al., 2021).).

The green synthesis of AgNPs using pineapple peel extract has been demonstrated in several prior studies. Das et al. (2019) reported the synthesis of AgNPs (10–20 nm) from A. comosus outer peel extract, demonstrating potent antioxidant, antibacterial, antidiabetic, and cytotoxic activities. Baran et al. (2021) synthesised spherical AgNPs (15–20 nm) derived from pineapple peel, which exhibited significant anticancer activity against HeLa and MCF-7 cancer cell lines. Mehrin et al. (2024) comprehensively characterised silver nanoparticles from pineapple and pomegranate peel extracts for bioelectrochemical applications. Despite these contributions, the systematic application of pineapple peel-derived AgNPs as adsorbents for slaughterhouse wastewater remediation, specifically targeting the kinetic profiles of colour, turbidity, and COD removal, has received very limited attention in the peer-reviewed literature.

Kinetic modelling of adsorption processes is indispensable for process design and scale-up, as it provides mechanistic insight into the rate-controlling steps, distinguishes between surface adsorption and diffusion-dominated mechanisms, and enables the calculation of rate constants necessary for reactor design (Hu et al., 2022). The pseudo-first-order (PFO), pseudo-second-order (PSO), and intraparticle diffusion (Weber–Morris) models are the kinetic frameworks most widely used for liquid-phase adsorption, each encoding distinct mechanistic assumptions that can be tested against experimental data (Largitte & Pasquier, 2016; Revellame et al.,2020).

Therefore, this study addresses a significant gap in the existing literature by: (i) synthesising and comprehensively characterising AgNPs from the aqueous extract of pineapple peel (AgPPE); (ii) treating SSW using AgPPE. (iii) Systematically evaluating the kinetics of colour, turbidity, and COD removal.

2.0. Materials and Methods

2.1. Chemicals and Reagents

All chemicals were analytical grade. Silver nitrate ($AgNO_3$, ≥99.8%), hydrochloric acid (HCl), sodium hydroxide (NaOH), nitric acid (HNO_3), and sulphuric acid (H_2SO_4) were obtained from Sigma-Aldrich (St. Louis, MO, USA). Deionised water (resistivity ≥18.2 MΩ·cm at 25 °C) and double-distilled water were used throughout all preparations and dilutions.

2.2. Collection and Preparation of the pineapple peel

Fresh pineapple (Ananas comosus) fruits were purchased from Eke Awka Market, Awka, Anambra State, Nigeria. The fruits were washed with running tap water and rinsed twice with deionised water. The peels were manually removed using clean stainless-steel tools and air-dried at ambient temperature (~28 °C) for 7

days to a constant weight. The dried peels were pulverised with an electric grinder and passed through a 0.5 mm mesh sieve to obtain a uniform particle size prior to extraction.

2.3. Preparation of Aqueous Extract from Pineapple Peel (PPE)

Two hundred (200) grams of dried and sieved pineapple peel powder were added to 500 mL deionised water in a 1000 mL flat-bottomed borosilicate flask and heated at 80 °C for 30 minutes with magnetic stirring at 300 rpm. After cooling to room temperature, the suspension was filtered through Whatman No. 1 filter paper to remove particulates. The resulting yellowish-green filtrate (PPE) was stored at 4 °C in sealed amber glass and used within 48 hours to minimise phytochemical degradation (Baran et al., 2021).

2.4. Biosynthesis of Silver Nanoparticles (AgPPE)

AgNPs were synthesised using the method of Baran et al. (2021) and Sengupta and Sarkar (2022) with moderate modifications. A fresh 0.1 M $AgNO_3$ solution was prepared immediately before use. Synthesis was initiated by the controlled dropwise addition of an $AgNO_3$ solution to PPE at a 1:4 (v/v) ratio (10 ml of $AgNO_3$: 40 ml of PPE) under continuous magnetic stirring at room temperature. The reaction vessel was wrapped in aluminium foil to exclude light. After 30 minutes of stirring, the mixture was incubated in the dark for 24 hours. The progressive change in colour from pale yellow to deep brownish-green (Figure 1) confirmed the bioreduction of Ag^+ to Ag^0. The suspension was centrifuged at 4,000 rpm for 45 minutes; the pellet was washed three times with deionised water by resuspension and recentrifugation to remove unreacted $AgNO_3$ and unbound biomolecules. The washed pellet was oven-dried at 60 °C for 12 hours, ground to obtain AgPPE powder, and stored in sealed amber glass vials until characterisation.

2.5. Physicochemical Characterization

UV–Vis optical absorption spectra were recorded using a UV-755B spectrophotometer (300–600 nm; deionised water as blank). FTIR spectra were acquired on a Shimadzu FTIR-8300 spectrophotometer (KBr pellet method; 4000–400 cm^{-1}; 4 cm^{-1} resolution; 32 scans averaged). TEM morphology and size were analysed using a JEM-2100 TEM (JEOL, Japan) at 200 kV; particle dimensions were measured from ≥100 particles using ImageJ. XRD powder diffraction was performed using a PANalytical XPERT-PRO diffractometer (Cu Kα radiation, λ = 1.5406 Å; 40 kV/40 mA; 2θ range 10°– 80°); average crystallite size was calculated using the Debye–Scherrer equation. EDX elemental analysis was performed with an Oxford Instruments Ultim Max Silicon Drift Detector. N_2 adsorption–desorption isotherms at 77 K were obtained with a Micromeritics TriStar II PLUS analyser; BET surface area and BJH pore size distribution were calculated from the data.

2.6. Collection and characterization of Slaughterhouse Wastewater

Slaughterhouse wastewater (SWW) was collected by composite grab sampling from an abattoir beside the New-Artisan River, New-Artisan, Independence Layout (Phase 2), Enugu, Enugu State, Nigeria (7°29'N, 7°30'E), following Nasiru et al. (2016) with modifications. The samples were collected in 20 L HDPE containers, pre-cleaned between 06:00 and 08:00 hours (peak slaughter), and transported to the laboratory in a cooler box. They were stored at 4 °C and filtered through Whatman No. 42 filter paper to remove coarse suspended matter before the experiments.

2.7. Batch Adsorption and Kinetic Experiments

Batch adsorption and kinetic experiments were conducted to determine the adsorption

efficiency and quantify the time-dependent removal of colour, turbidity, and COD from SWW by AgPPE. A known mass of 500 mg of AgPPE adsorbent was introduced into a container that holds 500 mL of SWW. The suspensions were agitated at 150 rpm on an orbital shaker at room temperature (~26 °C) and an initial pH of 7. At predetermined contact times of 0, 30, 60, 90, 105, 120, 150 and 180 min, aliquots were withdrawn, filtered through 0.45 µm membrane filters, and residual colour (UV–Vis spectrophotometry, Pt-Co method), Turbidity (nephelometry) and COD (closed reflux titrimetric method, APHA 5220C).

2.8. Adsorption Efficiency Calculations and Kinetic Modelling

2.8.1. Percentage Removal Efficiency

The percentage of adsorption efficiency (removal efficiency, %R) at each time point was calculated as:

$$\% R = \frac{Co - Ct}{Co} \times 100 \quad (1)$$

Where C_0 is the initial pollutant concentration and C_t is the residual concentration at time t.

2.8.2. Amount added at Time t

The amount of adsorbed adsorbate per unit mass of adsorbent at time t, q_t (mg/g) was calculated as follows:

$$q_t = \frac{Co - Ct}{M} \times V \quad (2)$$

Here, V (L) is the volume of the solution and m (g) is the mass of adsorbent employed.

2.8.3. Equilibrium Adsorption Capacity

The equilibrium adsorption capacity, q_e (mg/g), was obtained similarly at equilibrium (t_eq):

$$q_e = \frac{Co - Ce}{M} \times V \quad (3)$$

Here, Ce (in mg/L or NTU) is the equilibrium residual concentration.

2.8.4. Pseudo-First-Order (PFO) Kinetic Model

The linearised form of the pseudo-first-order kinetic equation is expressed as:

$$\log(qe - qt) = logqe - \left(\frac{k1}{2.303}\right) x\ t \quad (4)$$

Where k_1 (min^{-1}) is the constant of the PFO rate, obtained from the slope of the linear plot of $\log(q_e - q_t)$ versus t. The PFO model assumes that the rate of adsorption is proportional to the number of vacant surface sites and that adsorption is governed by external mass transfer (physisorption) (Alsharif, 2025).

2.8.5. Pseudo-Second Order (PSO) Kinetic Model

The linearised form of the pseudo-second-order kinetic equation is as follows:

$$\frac{t}{qt} = \frac{1}{k_2 qe^2} + \frac{t}{qe} \quad (5)$$

Where k_2 (g mg^{-1} min^{-1}) is the constant PSO rate. A linear plot of t/q_t versus t yields q_e from the slope ($1/q_e$) and k_2 from the intercept ($1/k_2 q_e^2$). The PSO model assumes chemisorption as the rate-determining step, with the rate proportional to the square of the number of unoccupied active sites (Alsharif, 2025). The initial sorption rate, h (mg g^{-1} min^{-1}), is given by:

$$h = k_2\ x\ qe^2 \quad (6)$$

2.8.6. Intraparticle Diffusion (Weber–Morris) Model

The intraparticle diffusion (IPD) model was applied to assess whether diffusion into the adsorbent pore structure contributes to rate control.

$$qt = k_i d\ x\ t^{0.5} + C \quad (7)$$

Where $k_i d$ (mg g^{-1} $min^{-0.5}$) is the intraparticle diffusion rate constant, and C (mg/g) is the intercept representing the boundary layer thickness. A linear plot of q_t versus $t^{0.5}$ with an

intercept C ≠ 0 indicates that the diffusion of the intraparticle is not the only rate-controlling step.

2.8.7. Boyd External Film Diffusion Model

The Boyd model was used to distinguish between external film diffusion and intraparticle diffusion as the rate control step (Wang & Guo, 2022).

$$F = \frac{qt}{qe} \quad (8)$$

$$Bt = -0.4977 - In(1 - F) \quad (9)$$

F is the fractional attainment of equilibrium at time t, and Bt is plotted against t; a straight line passing through the origin indicates intra-particle diffusion controls the rate, while a non-linear plot or a line not passing through the origin indicates film diffusion controls it

3.0. Results and Discussion

3.1. Characterization of AgPPE

3.1.1. Visual Observation and colour change

Upon mixing PPE with $AgNO_3$ solution, an induction period of ~10–15 min was observed, followed by a progressive change in colour from pale yellow → to golden-yellow → stable brownish-green over 20–60 min (Figure 1). This macroscopic change in colour is the most immediate evidence of AgNP formation, arising from the excitation of surface plasmon resonance (SPR) in the visible range (Ohiduzzaman et al., 2024). The brownish colour is characteristic of small-diameter spherical AgNPs (<20 nm) and has been reported for pineapple-derived AgNPs (Baran et al., 2021; Das et al., 2019). The colloid remained stable for >30 days during dark storage, indicating effective electrosteric stabilisation by the organic phytochemical corona of pineapple peel.

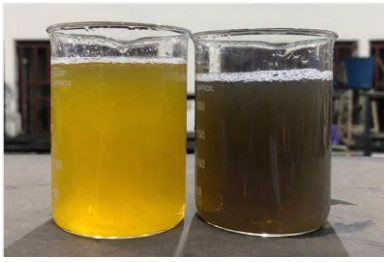

Figure 1: Change in colour during the synthesis of AgPPE from pineapple peel extract (left: initial pale yellow; right: final brownish-green after 24 h of incubation).

3.1.2. UV–Vis Spectroscopic Analysis

UV–Vis spectroscopy is a rapid, non-destructive, and widely used method for confirming AgNP formation (Asif et al., 2022). Surface plasmon resonance (SPR) arises from the collective oscillation of electrons in the conduction band in metallic nanoparticles under electromagnetic radiation (Demishkevich et al., 2023).

The UV–Vis spectrum of AgPPE (Figure 2) shows a sharp and symmetric SPR peak at 418 nm, within the typical 390–490 nm range for biogenically synthesised spherical AgNPs (Ohiduzzaman et al., 2024; Liu et al., 2015). The narrow FWHM (~65 nm) and the peak symmetry indicate a near-monodisperse size distribution with minimal aggregation (Mehrin et al., 2024). The lack of absorption above 500–550 nm further excludes significant agglomeration or anisotropy. These results agree with previous reports for A. comosus peel-derived AgNPs, which show SPR at 413 nm (Das et al., 2019) and 420 nm (Baran et al., 2021).

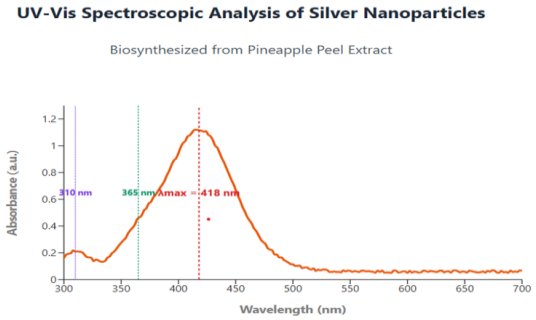

Figure 2: UV–Vis absorption spectrum of AgPPE.

3.1.3. FTIR Spectroscopic Analysis

FTIR spectroscopy identified the functional groups in pineapple peel that are involved in Ag^{+} bioreduction and AgPPE nanoparticle capping/stabilisation (Figure 3). The broad OH stretching band at 3200–3400 cm^{-1} is red-shifted relative to the free extract, indicating coordination of phenolic -OH with the Ag surface and confirming polyphenols as the main reductants (Ahmed et al., 2016). Bands at 2925 and 2850 cm^{-1} correspond to aliphatic C–H stretching. The strong C=O stretching at 1635–1650 cm^{-1} (Amide I) and N–H bending at 1560–1580 cm^{-1} (Amide II) show that proteinaceous biomolecules, including bromelain, act as capping agents (Alayande et al., 2025). C–O–C ether stretching at 1050–1100 cm^{-1} originates from polysaccharides (cellulose, pectin, hemicellulose) in the corona (Yusoff et al., 2020). The band at 420–450 cm^{-1}, assigned to the stretching of the Ag-O metal ligand, provides direct evidence of covalent bonding between the Ag core and the organic capping layer, confirming the formation of AgNPs (Baran et al., 2021; Rocha et al., 2024).

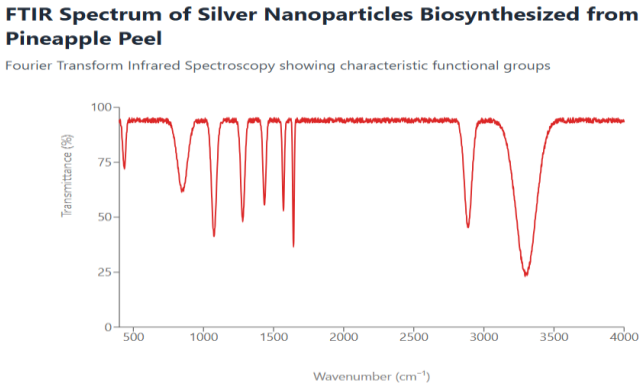

Figure 3: FTIR spectrum of AgPPE.

3.1.4. Transmission Electron Microscopic (TEM) Analysis

TEM directly visualised AgPPE morphology and size distribution (Figure 4). The micrograph shows predominantly spherical to oval nanoparticles, uniformly distributed with excellent dispersion. The diameters ranged from 14.62 to 17.63 nm (mean 16.1 ± 1.4 nm) with a quasi-Gaussian distribution, indicating narrow polydispersity. Minimal aggregation confirms effective electrosteric stabilisation by the biomolecular corona of the pineapple peel (Bélteky et al., 2021). The spherical morphology is thermodynamically favoured by the approximately isotropic phytochemical capping on growing Ag nuclei, which suppresses anisotropic growth (Vanlalveni et al., 2021). For adsorptive applications, <20 nm spherical particles offer a high surface-to-volume ratio and the maximum number of accessible active sites per unit mass (Rocha et al., 2024). These results agree with those of the AgNPs derived from pineapple peel reported by Baran et al. (2021) (15–20 nm) and Das et al. (2019) (12–18 nm).

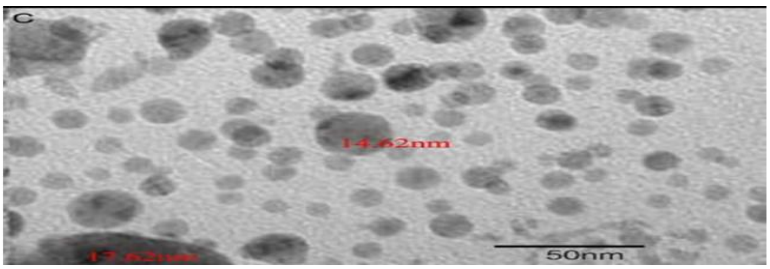

Figure 4: TEM micrograph of AgPPE.

3.1.5. X-ray Diffraction (XRD) Analysis

The reflections of gg at 2θ = 38.2°, 44.4°, 64.6 ° and 77.5°, indexed to the crystallographic planes (111), (200), (220) and (311) of the face-centred cubic phase (FCC) of metallic silver (JCPDS Card No. 04-0783; space group $Fm\bar{3}m$; a = 4.086 Å), unambiguously confirming the formation of crystalline zero-valent Ag^0 (Ali et al). The dominant (111) reflection indicates preferential crystal growth along the [111] direction, thermodynamically favoured for FCC metals. Critically, no silver oxide phases (Ag_2O or AgO) were detected, confirming complete bioreduction and phase purity of AgPPE. Application of the Debye–Scherrer equation (Eq. 10) below to the (111) peak yielded an average crystallite size D ≈ 20.4 nm. The slightly larger XRD crystallite size relative to TEM measurements (14.62–17.63 nm) is expected for polycrystalline particles, in which X-ray coherent scattering domains may span multiple crystallographic units (Mehrin et al., 2024). These findings are consistent with the values in the literature for AgNPs derived from A. comosus peel (Baran et al., 2021; Das et al., 2019).

$$D = \frac{k\lambda}{\mathrm{bcosq}} \qquad (10)$$

Where D is the average crystalline size of the nanoparticles, k is the geometric factor (0.9), λ is the wavelength of X-ray radiation source, and b is the angular full-width at half maximum (FWHM, i.e., Full Width at Half Maximum) of the XRD peak at the diffraction angle.

Anachem Journal, 17(1), 38-60
DOI: https://doi.org/10.5281/zenodo.20128534

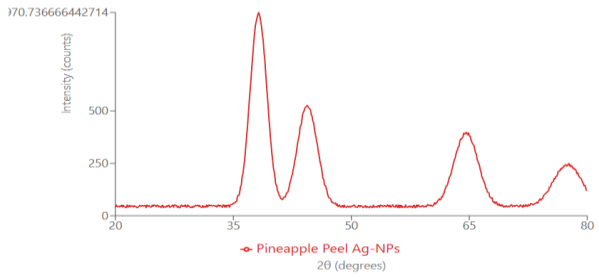

Figure 5: XRD diffractogram of AgPPE.

3.1.6. Energy-Dispersive X-ray (EDX) Analysis

EDX spectroscopy confirmed elemental silver as the dominant constituent of AgPPE (60.16 wt%, 42.51 at%), with a characteristic Lα emission peak at 3.05 keV (Figure 6 below). Additional signals from C (21.83 wt%), O (10.45 wt%), N (3.91 wt%), and Cl (3.65 wt%) originate from the organic biomolecular corona (polyphenols, bromelain, pectin) adsorbed on the nanoparticle surface (Baran et al., 2021; Ahmed et al., 2016). The nitrogen signal corroborates the presence of proteinaceous capping biomolecules (Khatami *et al.,* 2021). No signals from metallic impurities were detected, confirming elemental purity and the selectivity of pineapple peel-mediated bioreduction.

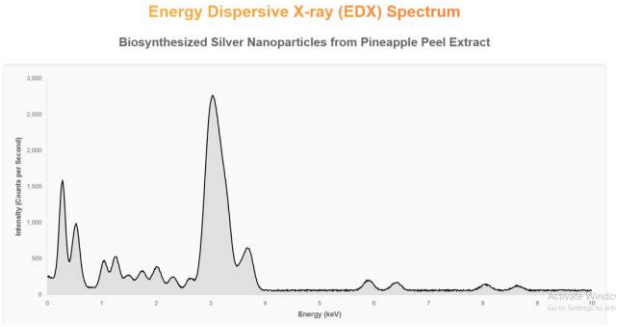

Figure 6: EDX spectrum of AgPPE.

3.1.7. BET Surface Area and Porosity Analysis

The N2 adsorption-desorption isotherms at 77 K (Figures 7–8) classified AgPPE as a Type II mesoporous material with an H3-type hysteresis loop (IUPAC classification), characteristic of slit-shaped mesopores in aggregated nanoparticle assemblies (Thommes et al., 2015). The linear plot of the BET (Figure 7 below) showed excellent linearity (R^2 = 0.9975) over the P/P_0 range of 0.05 to 0.30, confirming the applicability of the BET model. BET analysis yielded a specific surface area of 449.842 m^2/g, total pore volume 0.285 cm^3/g (micropore volume 0.058 cm^3/g; mesopore volume 0.227 cm^3/g), and mean BJH pore diameter 2.53 nm. This extraordinarily high surface area, several orders of magnitude above bulk silver (≤1 m^2/g), is a direct consequence of the nanoscale particle dimensions and inter-particle void structure. These textural properties constitute the primary structural basis for the observed high adsorption capacities of AgPPE (Channei & Manuspiya, 2025; Ghapar et al., 2024).

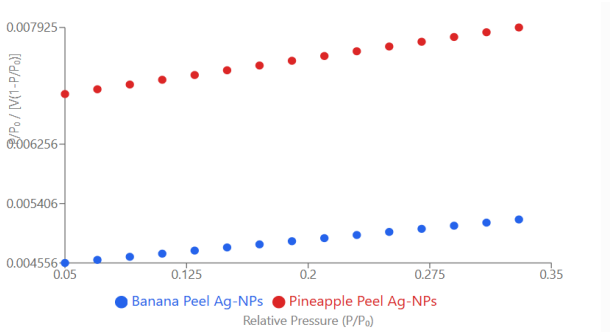

Figure 7: BET linear plot for N_2 adsorption on AgPPE, confirming model applicability (R^2 = 0.9975) over P/P_0 = 0.05–0.30.

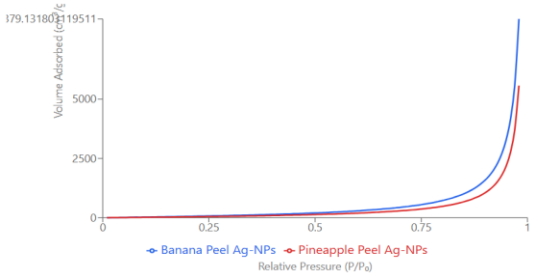

Figure 8. N_2 adsorption–desorption isotherm of AgPPE at 77 K, showing Type II IUPAC classification with H3-type hysteresis loop, characteristic of mesoporous character.

3.2. Concentration–Time Profiles for AgPPE Adsorption

The concentration–time (C vs t) profiles for colour, turbidity, and COD removal by AgPPE are presented in Figure 9. All three pollutant concentration profiles exhibit a characteristic biphasic decline: a rapid initial decrease during the early phase (0–90 min), followed by a progressively slower decline, culminating in approximate equilibrium plateaus at 90–105 min. For colour, the initial concentration of 207.5 mg/L declined sharply to 131.0 mg/L at 30 min, then to 51.5 mg/L at 105 min (75.18% removal). Turbidity decreased from 255 NTU to 68.4 NTU at 90 min (72.94% removal), achieving equilibrium slightly earlier than colour and COD. COD declined from 550 mg/L to 158.5 mg/L at 105 min (71.27% removal).

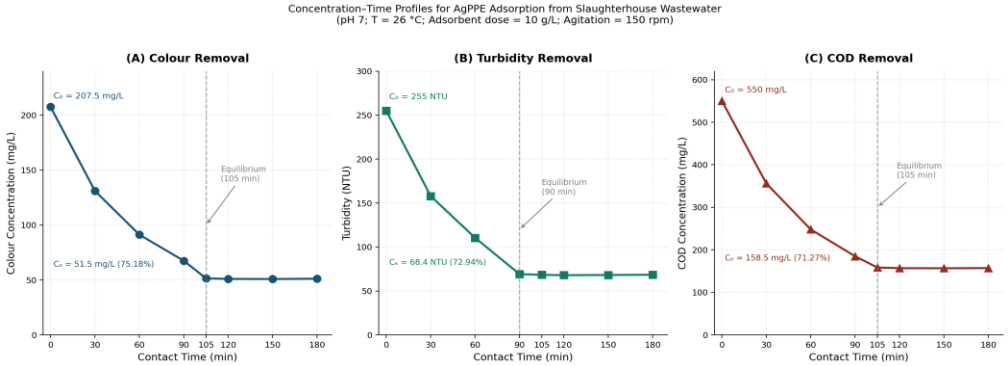

Figure 9: Concentration–time profiles for the removal of (A) Colour, (B) Turbidity, and (C) COD. Dashed vertical lines indicate equilibrium contact time.

The biphasic kinetic profiles are mechanistically attributable to: (i) an initial rapid phase driven by abundant unoccupied surface active sites and high concentration gradient between solution and adsorbent, providing a strong driving force for mass transfer; and (ii) a slower second phase governed by gradual saturation of accessible surface sites, increased electrostatic repulsion among adsorbed species, and diffusion-limited uptake through mesoporous channels (Largitte & Pasquier, 2016). The earlier equilibrium for turbidity (90 min) relative to colour and COD (105 min) indicates that particulate turbidity-contributing matter is adsorbed more readily, consistent with predominantly surface-mediated physical capture, while dissolved organic chromophores and COD-contributing species require diffusion into internal pore structures (Azeez et al., 2018). These observations are consistent with previous studies on complex wastewater adsorption, confirming that the process proceeds via a multi-stage mechanism involving surface adsorption followed by diffusion-controlled uptake (Al-Harby et al., 2021).

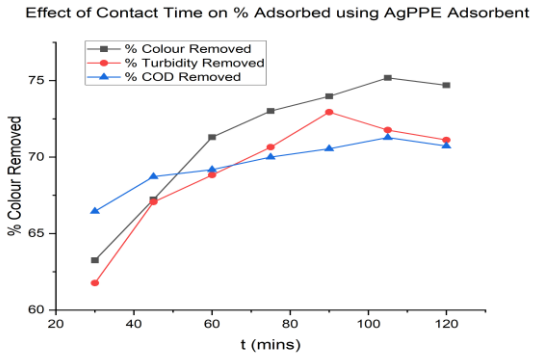

Figure 10: Effect of contact time on percentage adsorption of Colour, Turbidity, and COD by AgPPE from slaughterhouse wastewater.

3.3. Adsorption Kinetic Modelling

Kinetic modelling was applied to elucidate the mechanism and rate-controlling steps governing AgPPE adsorption from SWW. The pseudo-first-order (PFO), pseudo-second-order (PSO), Weber–Morris intraparticle diffusion (IPD), and Boyd models were applied to kinetic data for colour, turbidity, and COD removal. Model parameters and goodness-of-fit statistics are summarised in Table 1.

3.3.1 Pseudo-First-Order (PFO) Model

The PFO model (Eq. 4) was fitted by plotting $\log(q_e - q_t)$ versus t. The linearised PFO plots for colour, turbidity, and COD adsorption onto AgPPE are shown in Figures 11, 12, and 13, respectively.

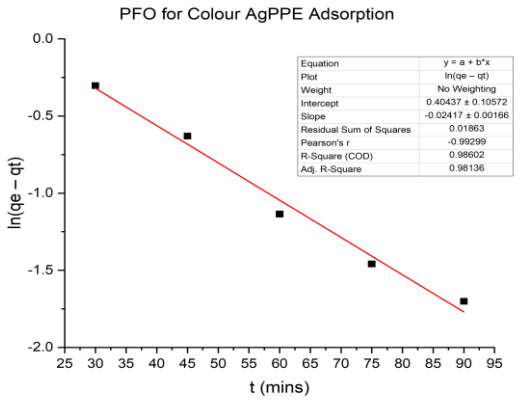

Figure 11. Pseudo-First-Order kinetic plot for AgPPE Colour adsorption from slaughterhouse wastewater.

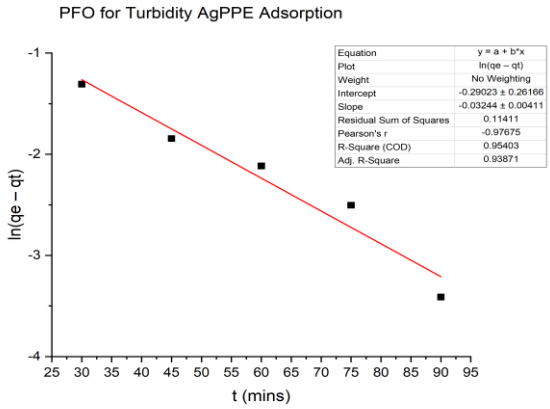

Figure 12. Pseudo-First-Order kinetic plot for AgPPE Turbidity removal from slaughterhouse wastewater.

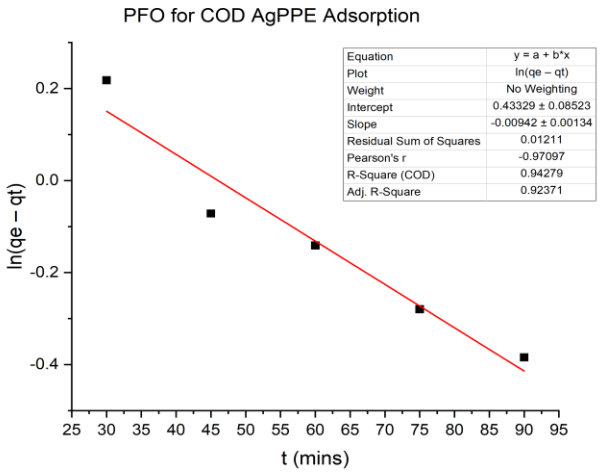

Figure 13. Pseudo-First-Order kinetic plot for AgPPE COD removal from slaughterhouse wastewater.

The PFO model yielded R^2 values of 0.986 (Colour), 0.954 (Turbidity), and 0.943 (COD). While individually satisfactory, these are substantially lower than PSO model values. More critically, the PFO-calculated q_e values (1.498, 0.748, and 1.542 mg/g for colour, Turbidity, and COD, respectively) deviate considerably from the experimentally observed q_e values (4.020, 1.583, and 10.381 mg/g), indicating that the PFO model severely underpredicts equilibrium capacity and does not adequately describe the adsorption mechanism. Correspondingly high χ^2 values (4.240, 0.931, and 50.650 for colour, turbidity, and COD) further confirm the inadequacy of the PFO model (Jain et al., 2020). The PFO model's assumption that the rate is proportional to the availability of vacant sites under dilute-solution conditions is insufficient to capture the dominant chemisorption mechanism governing AgPPE-SWW interactions.

3.3.2. Pseudo-Second-Order (PSO) Model

The PSO model (Eq. 5) was linearised as t/q_t versus t. The PSO plots for colour, turbidity, and COD adsorption onto AgPPE are shown in Figures 14, 15, and 16, respectively.

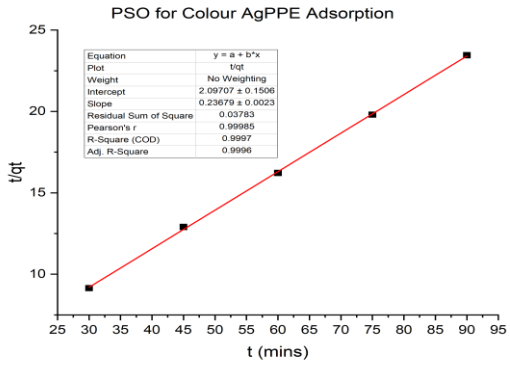

Figure 14. Pseudo-Second-Order kinetic plot for AgPPE Colour adsorption from slaughterhouse wastewater.

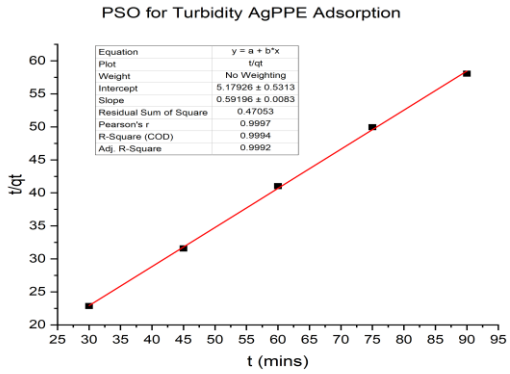

Figure 15. Pseudo-Second-Order kinetic plot for AgPPE Turbidity removal from slaughterhouse wastewater.

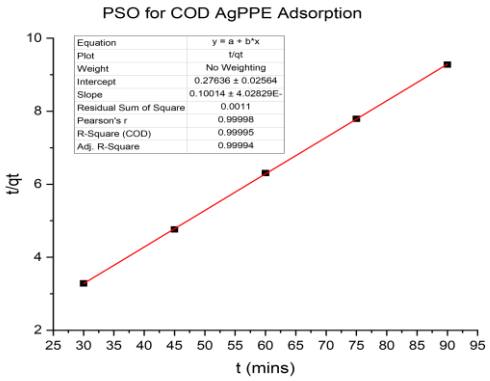

Figure 16. Pseudo-Second-Order kinetic plot for AgPPE COD removal from slaughterhouse wastewater.

The PSO model produced exceptional fits for all three pollutant parameters: R^2 = 0.9997 (colour), 0.999 (turbidity), and 0.99995 (COD), with extremely low χ^2 values of 0.010, 0.007, and 0.015 respectively, establishing the PSO model as the definitive kinetic descriptor. Furthermore, PSO-calculated q_e values (4.220, 1.689, and 10.000 mg/g) correspond closely to the experimentally observed values (4.020, 1.583, and 10.381 mg/g), validating the physical meaningfulness of the model parameters. The PSO rate constants k_2 were 0.027 g mg^{-1} min^{-1} (tolour), 0.068 g mg^{-1} min^{-1} (turbidity), and 0.036 g mg^{-1} min^{-1} (COD). The initial sorption rate h (Eq. 6) was 0.481 mg g^{-1} min^{-1} (colour), 0.193 mg g^{-1} min^{-1} (turbidity), and 3.600 mg g^{-1} min^{-1} (COD).

The superiority of the PSO model confirms that chemisorption is the rate-determining step in AgPPE adsorption from SWW. Chemisorption involves the formation of strong, site-specific bonds between adsorbate molecules and functional groups on the AgPPE surface, specifically between electron-rich chromophoric and organic compounds in SWW and silver atoms, as well as between organic adsorbates and hydrogen-bonding/coordinating functional groups (–OH, –COOH, $–NH_2$) of the phytochemical corona (Beni & Esmaeili, 2020). This interpretation is entirely consistent with FTIR evidence of multiple functional groups on AgPPE that are capable of chemisorptive interactions. The PSO model has been widely reported as the dominant kinetic descriptor for adsorption of organic pollutants and colour from complex wastewaters onto biogenic nanomaterial adsorbents (Azeez et al., 2018; Al-Qahtani, 2017).

3.3.3. Intraparticle Diffusion (IPD) Model

Weber–Morris IPD plots (q_t vs. $t^{0.5}$; Eq. 7) for AgPPE are shown in Figures 17–19.

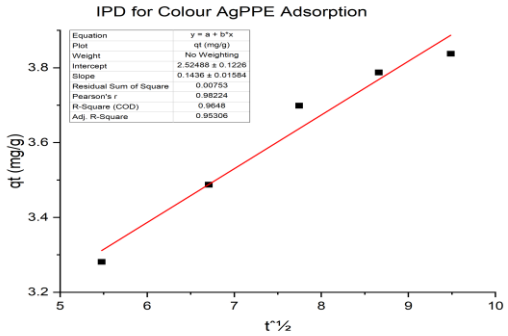

Figure 17. Intraparticle diffusion (Weber–Morris) plot for AgPPE Colour adsorption from slaughterhouse wastewater.

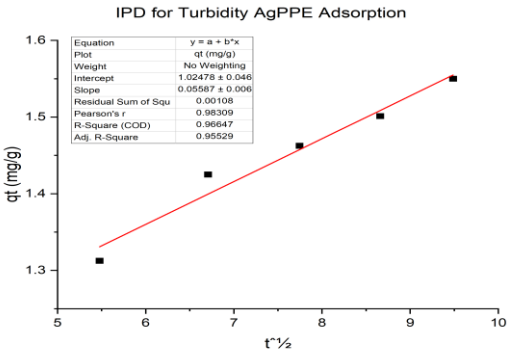

Figure 18. Intraparticle diffusion (Weber–Morris) plot for AgPPE Turbidity removal from slaughterhouse wastewater.

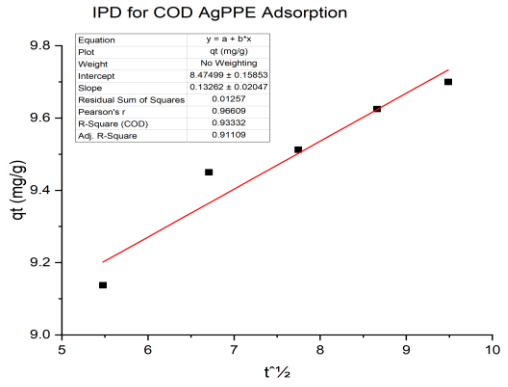

Figure 19. Intraparticle diffusion (Weber–Morris) plot for AgPPE COD removal from slaughterhouse wastewater.

The IPD model yielded Kid values of 0.144 (colour), 0.056 (turbidity), and 0.133 mg g^{-1} $min^{-0.5}$ (COD), with non-zero positive intercepts C of 2.525, 1.025, and 8.475 mg/g, respectively. The R^2 values (0.965, 0.966, 0.933) indicate adequate but imperfect linear fits. The nonzero C intercepts representing the boundary-layer-thickness contribution unambiguously indicate that intraparticle diffusion is a contributing factor but not the sole rate-controlling step. External film diffusion and surface adsorption also contribute to the overall uptake rate, as is typical for mesoporous adsorbents with hierarchical pore structures (Wang & Guo, 2022).

3.3.4. Boyd Film Diffusion Model

Boyd plots (Bt vs. t; Eqs. 8–9) for AgPPE are shown in Figures 20–22.

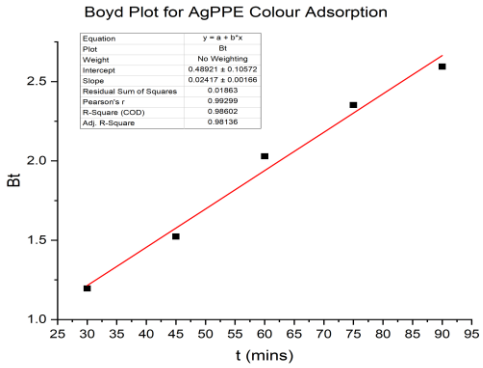

Figure 20. Boyd plot for AgPPE Colour adsorption from slaughterhouse wastewater.

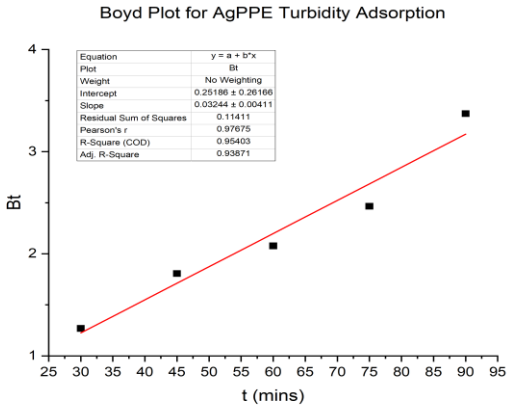

Figure 21. Boyd plot for AgPPE Turbidity removal from slaughterhouse wastewater.

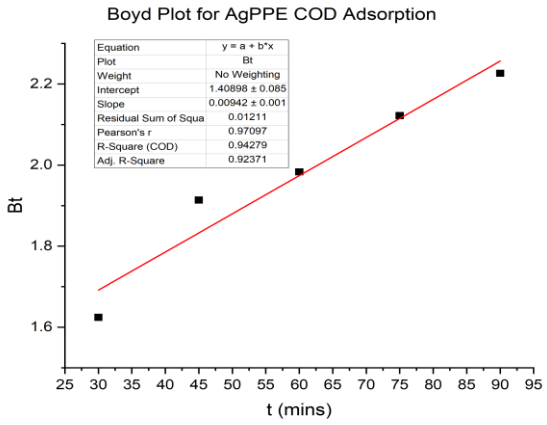

Figure 22. Boyd plot for AgPPE COD removal from slaughterhouse wastewater.

Boyd plots for all three parameters were linear but did not pass through the origin (positive y-intercepts), confirming that external film diffusion at the adsorbent–solution interface constitutes an additional rate-limiting step alongside intra-particle diffusion (Wang & Guo, 2022). This mechanistic picture is consistent with the adsorption of a complex multi-component wastewater, where the diverse molecular sizes and chemical functionalities of SWW constituents impose diffusion resistances across both the external boundary layer and the internal pore channels of mesoporous AgPPE.

Table 1. Summary of kinetic modelling parameters for Colour, Turbidity, and COD adsorption from slaughterhouse wastewater onto AgPPE.

Model	Parameter	AgPPE Colour	AgPPE Turbidity	AgPPE COD
PFO	*qe,exp (mg/g)*	4.020	1.583	10.381
	qe,calc (mg/g)	1.498	0.748	1.542
	k_1 *(min^{-1})*	0.024	0.032	0.009
	R^2	0.986	0.954	0.943
	χ^2	4.240	0.931	50.650
PSO	*qe,calc (mg/g)*	4.220	1.689	10.000
	k_2 *(g mg^{-1} min^{-1})*	0.027	0.068	0.036

Model	Parameter	AgPPE Colour	AgPPE Turbidity	AgPPE COD
	R^2	0.9997	0.999	0.99995
	χ^2	0.010	0.007	0.015
IPD	*Kid (mg* g^{-1} $min^{-0.5}$*)*	0.144	0.056	0.133
	C (mg/g)	2.525	1.025	8.475
	R^2	0.965	0.966	0.933

3.4. Proposed Adsorption Mechanism

Based on converging evidence from kinetic modelling, characterization data, and BET textural analysis, the following integrated adsorption mechanism is proposed for the AgPPE-mediated removal of colour, turbidity, and COD from SWW. The process proceeds in three sequential stages: (i) External mass transfer: SWW pollutant molecules migrate from the bulk solution through the stagnant hydrodynamic boundary layer surrounding AgPPE agglomerates to the external nanoparticle surface, driven by the concentration gradient; Boyd plot analysis confirms that film diffusion resistance is operative. (ii) Surface chemisorption: colour-contributing chromophores, colloidal turbidity particles, and COD-contributing organics adsorb onto the AgPPE surface through π–π stacking of aromatic chromophores with phenolic ring systems in the phytochemical corona; hydrogen bonding between –OH, –COOH, and $–NH_2$ groups in the corona and polar functional groups of SWW organics; Lewis acid–base coordination between surface Ag atoms and electron-donating groups of SWW molecules; and electrostatic attraction between the charged AgPPE surface and oppositely charged organic species. PSO kinetic dominance ($R^2 \geq 0.9997$) confirms chemisorption as the principal rate-determining step. (iii) Intraparticle diffusion: Following external surface saturation, adsorbate molecules diffuse into the mesoporous interior via the 2.53 nm pore channels, accessing the large internal surface area (449.842 m^2/g). The non-zero IPD model intercept confirms contribution of this stage without it being the sole rate-controlling mechanism.

4. Conclusions

This study has demonstrated the successful green synthesis of silver nanoparticles (AgPPE) from aqueous pineapple peel (*Ananas comosus*) extract, and their effective application as nanomaterial adsorbents for the simultaneous removal of colour, turbidity, and COD from real slaughterhouse wastewater. Multi-technique characterization confirmed the formation of high-purity, crystalline, mesoporous, spherical AgNPs (14.62–17.63 nm; BET surface area 449.842 m^2/g) capped by a multi-component pineapple peel phytochemical coron**a**.

Initial characterization of the SWW established: COD = 550 mg/L, Colour = 207.5 mg/L (Pt-Co units, measured spectrophotometrically), and Turbidity = 255 NTU (measured by nephelometry). These values substantially exceed NESREA effluent discharge guidelines and confirmed the

necessity of treatment (NESREA, 2011). Batch kinetic experiments established equilibrium at 90 min (Turbidity) and 105 min (colour and COD), with maximum removals of 156.00 mg/L for Colour (75.18%, residual 51.50 mg/L), 185.99 NTU for Turbidity (72.94%, residual 69.01 NTU), and 391.99 mg/L for COD (71.27%, residual 158.01 mg/L); the residual values were well below the NESREA effluent discharge standard. Pseudo-second-order kinetics provided the definitive fit to all three pollutant datasets ($R^2 \geq 0.9997$; $\chi^2 \leq 0.015$), confirming chemisorption as the rate-determining mechanism. Intraparticle diffusion was a contributing factor, and Boyd plot analysis confirmed concurrent external film diffusion resistance. Concentration–time profiles quantitatively captured the biphasic dynamics of pollutant removal.

These findings establish AgPPE as a green, sustainable, and effective nanomaterial for multi-parameter remediation of complex agro-industrial wastewater. Future investigations should address isotherm modelling, thermodynamic parameters, adsorbent regeneration, and pilot-scale evaluation to advance AgPPE towards practical deployment in wastewater treatment.

Ethical Approval

Not applicable. This study does not involve human subjects or animal experiments.

REFERENCES

Abid, N., Khan, A. M., Shujait, S., Chaudhary, K., Ikram, M., Imran, M., Haider, J., Khan, M., Khan, Q., & Maqbool, M. (2022). Synthesis of nanomaterials using various top-down and bottom-up approaches, influencing factors, advantages, and disadvantages: A review. *Advances in Colloid and Interface Science,* 300, 102597. https://doi.org/10.1016/j.cis.2021.102597

Ahmed, S., Ahmad, M., Swami, B. L., & Ikram, S. (2016). A review on plants extract mediated synthesis of silver nanoparticles for antimicrobial applications: A green expertise. *Journal of Advanced Research,* 7(1), 17–28. https://doi.org/10.1016/j.jare.2015.02.007

Ahmed, S., Mofijur, M., Nuzhat, S., Chowdhury, A. T., Rafa, N., Uddin, M. A., Inayat, A., Mahlia, T. M. I., Ong, H. C., Fattah, I. M. R., & Show, P. L. (2021). Recent developments in physical, biological, chemical, and hybrid treatment techniques for removing emerging contaminants from wastewater. *Journal of Hazardous Materials,* 416,125912.https://doi.org/10.1016/j.jhazmat. 2021.125912

Alayande, A. B., Obayomi, K. S., & Park, H. (2025). Green biosynthesis and antimicrobial activity of silver nanoparticles synthesized by Lactobacillus acidophilus against multidrug-resistant Klebsiella pneumoniae. *BMC Biotechnology,* 25, 8. https://doi.org/10.1186/s12896-025-01018-9

Al-Ghouti, M. A., & Da'ana, D. A. (2020). Guidelines for the use and interpretation of adsorption isotherm models: A review. *Journal of Hazardous Materials,* 393, 122383. https://doi.org/10.1016/j.jhazmat.2020.122383

Al-Harby, N. F., Albahly, E. F., & Mohamed, N. A. (2021). Kinetics, isotherm and thermodynamic studies for efficient adsorption of Congo red dye from aqueous solution onto novel cyanoguanidine-modified chitosan adsorbent. *Polymers,* 13(24), 4446. https://doi.org/10.3390/polym13244446

Ali, M. H., Azad, M. A. K., Khan, K. A., Rahman, M. O., Chakma, U., & Kumer, A. (2023). Analysis of crystallographic structures and properties of silver nanoparticles synthesized using PKL extract and nanoscale

characterization techniques. *ACS Omega,* 8(31), 28133–28142. https://doi.org/10.1021/acsomega.3c01261

Al-Qahtani, K. M. (2017). Cadmium removal from aqueous solution by green synthesis zero valent silver nanoparticles with Benjamina leaves extract. *The Egyptian Journal of Aquatic Research,* 43(4), 269–274. https://doi.org/10.1016/j.ejar.2017.10.003

Alsharif, M. A. (2025). Understanding adsorption: Theories, techniques, and applications. In Adsorption—Fundamental mechanisms and applications. *IntechOpen.* https://doi.org/10.5772/intechopen.1008865

Ang, W. L., & Mohammad, A. W. (2020). State of the art and sustainability of natural coagulants in water and wastewater treatment. *Journal of Cleaner Production,* 262, 121267. https://doi.org/10.1016/j.jclepro.2020.121267

Asif, M., Yasmin, R., Asif, R., Ambreen, A., Mustafa, M., & Umbreen, S. (2022). Green synthesis of silver nanoparticles (AgNPs), structural characterization, and their antibacterial potential. Dose-Response, 20(2), 15593258221088709.

Aziz, A., Basheer, F., Sengar, A., Irfanullah, Khan, S. U., & Farooqi, I. H. (2019). Biological wastewater treatment (anaerobic-aerobic) technologies for safe discharge of treated slaughterhouse and meat processing wastewater. *Science of the Total Environment,* 686,681–708.https://doi.org/10.1016/j.scitotenv.2019.05.295

Azeez, L., Lateef, A., Adebisi, S. A., & Oyedeji, A. O. (2018). Novel biosynthesized silver nanoparticles from cobweb as adsorbent for Rhodamine B: Equilibrium isotherm, kinetic and thermodynamic studies. *Applied Water Science,* 8(1), 32. https://doi.org/10.1007/s13201-018-0676-z

Baran, A., Keskin, C., Baran, M. F., Huseynova, I., Khalilov, R., Eftekhari, A., Irtegun-Kandemir, S., & Kavak, D. E. (2021). Ecofriendly synthesis of silver nanoparticles using Ananas comosus fruit peels: Anticancer and antimicrobial activities. *Bioinorganic Chemistry and Applications,* 2021, 2058149. https://doi.org/10.1155/2021/2058149

Bélteky, P., Rónavári, A., Zakupszky, D., Boka, E., Igaz, N., Szerencsés, B., Pfeiffer, I., Vágvölgyi, C., Kiricsi, M., & Kónya, Z. (2021). Are smaller nanoparticles always better? Understanding the biological effect of size-dependent silver nanoparticle aggregation under biorelevant conditions. *International Journal of Nanomedicine,* 16, 3021–3040.

Beni, A. A., & Esmaeili, A. (2020). Biosorption, an efficient method for removing heavy metals from industrial effluents: A review. *Environmental Technology & Innovation,* 17, 100503. https://doi.org/10.1016/j.eti.2019.100503

Bustillo-Lecompte, C. F., & Mehrvar, M. (2015). Slaughterhouse wastewater characteristics, treatment, and management in the meat processing industry: A review on trends and advances. *Journal of Environmental Management,* 161, 287–302. https://doi.org/10.1016/j.jenvman.2015.07.008

Channei, D., & Manuspiya, H. (2025). From waste to value: Banana-peel-derived adsorbents for water treatment. *Applied Sciences,* 15(4), 2205. https://doi.org/10.3390/app15042205

Crini, G., & Lichtfouse, E. (2019). Advantages and disadvantages of techniques used for wastewater treatment. *Environmental Chemistry Letters,* 17(1), 145–155. https://doi.org/10.1007/s10311-018-0785-9

Crini, G., Lichtfouse, E., Wilson, L. D., & Morin-Crini, N. (2019). Conventional and non-conventional adsorbents for wastewater

treatment. *Environmental Chemistry Letters,* 17(1), 195–213. https://doi.org/10.1007/s10311-018-0786-y

Das, G., Patra, J. K., Debnath, T., Ansari, A., & Shin, H. S. (2019). Investigation of antioxidant, antibacterial, antidiabetic, and cytotoxicity potential of silver nanoparticles synthesized using the outer peel extract of Ananas comosus (L.). *PLoS ONE,* 14(8), e0220950. https://doi.org/10.1371/journal.pone.0220950

Deshmukh, S. P., Patil, S. M., Mullani, S. B., & Delekar, S. D. (2019). Silver nanoparticles as an effective disinfectant: A review. *Materials Science and Engineering: C, 97*, 954–965. https://doi.org/10.1016/j.msec.2018.12.102

Demishkevich, E., Zyubin, A., Seteikin, A., Samusev, I., Park, I., Hwangbo, C. K., Choi, E. H., & Lee, G. J. (2023). Synthesis methods and optical sensing applications of plasmonic metal nanoparticles made from rhodium, platinum, gold, or silver. Materials, 16(9), 3342. https://doi.org/10.3390/ma16093342

Eze, C. N., & Eze, P. C. (2018). Effect of abattoir waste on the physicochemical and bacteriological qualities of New-Artisan River in Enugu, Nigeria. Nigerian Journal of Technology, 37(1), 262–267. https://doi.org/10.4314/njt.v37i1.34

Food and Agriculture Organization of the United Nations. (2022). FAOSTAT: Crops and livestock products. https://www.fao.org/faostat/

Ghapar, N. F. A., Abu Samah, R., Abdul Wahab, M. S., Abd Rahman, S., & Othman, M. H. D. (2024). An insight into pineapple peel waste adsorbent for iron-contaminated water through kinetic and isotherm study. *Malaysian Journal of Analytical Sciences, 28*(2), 397–411.

Güzel, R., & Erdal, G. (2018). Synthesis of silver nanoparticles. In Silver nanoparticles: Fabrication, characterization and applications. *IntechOpen.*https://doi.org/10.5772/intechopen.75363

Hu, Q., Pang, S., & Wang, D. (2022). In-depth insights into mathematical characteristics, selection criteria and common mistakes of adsorption kinetic models: A critical review. *Separation & Purification Reviews,* 51(3), 281–299. https://doi.org/10.1080/15422119.2021.1922444

Jain, K., Patel, A. S., Pardhi, V. P., & Flora, S. J. S. (2021). Nanotechnology in wastewater management: A new paradigm towards wastewater treatment. *Molecules,* 26(6), 1797. https://doi.org/10.3390/molecules26061797

Jain, M., Yadav, M., Kohout, T., Lahtinen, M., Garg, V. K., & Sillanpää, M. (2020). Development of iron oxide/activated carbon nanoparticle composite for the removal of heavy metal ions from aqueous solution. Water Resources and Industry, 20, 54–74. https://doi.org/10.1016/j.wri.2018.09.001

Khatami, M., Alijani, H. Q., Heli, H., & Sharifi, I. (2021). Green synthesized silver nanoparticles: Antibacterial and anticancer activities, biocompatibility, and analyses of surface-attached proteins. *Frontiers in Microbiology,* 12, 632505. https://doi.org/10.3389/fmicb.2021.632505

Largitte, L., & Pasquier, R. (2016). A review of the kinetics adsorption models and their application to the adsorption of lead by an activated carbon. *Chemical Engineering Research and Design,* 109, 495–504. https://doi.org/10.1016/j.cherd.2016.02.006

Liu, X., Li, D., Sun, X., Li, Z., Song, B., Sun, H., & Jiang, H. (2015). Tunable dipole surface plasmon resonances of silver nanoparticles by

cladding dielectric layers. *Scientific Reports,* 5(1),12555. https://doi.org/10.1038/srep12555

Lu, C., & Astruc, D. (2018). Nanomaterials for removal of toxic elements from water. *Coordination Chemistry Reviews,* 356, 147–164. https://doi.org/10.1016/j.ccr.2017.11.003

Mehrin, S., Tanisa, N. Y., Awal, R., Alam Khan, M. K., Shaqur, A., Ahmed, S., & Mia, A. (2024). Efficient bioelectrochemical cell generation and green synthesis of silver nanoparticles using pomegranate and pineapple peel extracts: A comprehensive characterization study. *Advances in Materials Science and Engineering,* 2024, 6681559.

Mekonnen, M. M., & Hoekstra, A. Y. (2016). Four billion people facing severe water scarcity. *Science Advances,* 2(2), e1500323. https://doi.org/10.1126/sciadv.1500323

Mohammed, M. A., Abubakar, B. I., & Kurna, B. B. (2017). Equilibrium and kinetic studies of adsorption of safranin-O from aqueous solutions using pineapple peels. Arid Zone *Journal of Engineering, Technology and Environment,* 13(6), 671–687.

Nasiru, A., Osakwe, C. E., Lawal, I. M., & Chinade, A. U. (2016). Assessment of physicochemical parameters and heavy metals in Gombe abattoir wastewater. American *Journal of Engineering Research,* 5, 64–69.

National Environmental Standards and Regulations Enforcement Agency. (2011). National environmental (surface and groundwater quality control) regulations, 2011. Federal Republic of Nigeria Official Gazette, 98(49), S.I. No. 22.

Ohiduzzaman, M., Khan, M. N. I., Khan, K. A., & Paul, B. (2024). Biosynthesis of silver nanoparticles by banana pulp extract: Characterizations, antibacterial activity, and bioelectricity generation. *Heliyon,* 10(3), e25520. https://doi.org/10.1016/j.heliyon.2024.e25520

Rehman, R., Farooq, S., & Mahmud, T. (2019). Use of agro-waste *Musa acuminata* and *Solanum tuberosum* peels for economical sorptive removal of emerald green dye in ecofriendly way. *Journal of Cleaner Production,* 206, 819–826. https://doi.org/10.1016/j.jclepro.2018.09.226

Revellame, E. D., Fortela, D. L., Sharp, W., Hernandez, R., & Zappi, M. E. (2020). Adsorption kinetic modeling using pseudo-first order and pseudo-second order rate laws: A review. *Cleaner Engineering and Technology,* 1, 100032. https://doi.org/10.1016/j.clet.2020.100032

Rocha, V., Ferreira-Santos, P., Aguiar, C., Neves, I. C., & Tavares, T. (2024). Valorization of plant by-products in the biosynthesis of silver nanoparticles with antimicrobial and catalytic properties. *Environmental Science and Pollution Research,* 31(9), 14191–14207. https://doi.org/10.1007/s11356-024-32180-w

Sengupta, A., & Sarkar, A. (2022). Synthesis and characterization of nanoparticles from neem leaves and banana peels: A green prospect for dye degradation in wastewater. *Ecotoxicology,* 31(4), 537–548. https://doi.org/10.1007/s10646-021-02414-5

Thommes, M., Kaneko, K., Neimark, A. V., Olivier, J. P., Rodriguez-Reinoso, F., Rouquerol, J., & Sing, K. S. W. (2015). Physisorption of gases, with special reference to the evaluation of surface area and pore size distribution (IUPAC Technical Report). *Pure and Applied Chemistry,* 87(9–10), 1051–1069. https://doi.org/10.1515/pac-2014-1117

Vanlalveni, C., Lallianrawna, S., Biswas, A., Selvaraj, M., Changmai, B., & Rokhum, S. L. (2021). Green synthesis of silver nanoparticles using plant extracts and their antimicrobial

activities: A review of recent literature. *RSC Advances,* 11(5), 2804–2837. https://doi.org/10.1039/d0ra09941d

Wang, J., & Guo, X. (2022). Rethinking of the intraparticle diffusion adsorption kinetics model: Interpretation, solving methods and applications. *Chemosphere,* 309, 136732. https://doi.org/10.1016/j.chemosphere.2022.136732

Yusoff, A. H., Mohammad, R., Mohamad, M., Sulaiman, A. Z., Che Zaudin, N. A., Rosmadi, N., & Teo, P. T. (2020). Potential of agricultural waste material (Ananas comosus) as biosorbent for heavy metal removal in polluted water. *Materials Science Forum,* 1010, 489–494. https://doi.org/10.4028/www.scientific.net/MSF.1010.489

Zhang, X. F., Liu, Z. G., Shen, W., & Gurunathan, S. (2016). Silver nanoparticles: Synthesis, characterization, properties, applications, and therapeutic approaches. International *Journal of Molecular Sciences,* 17(9),1534.https://doi.org/10.3390/ijms17091534